Aerosol Science and Technology, 39:902–911, 2005

ISSN: 0278-6826 print / 1521-7388 online
DOI: 10.1080/02786820500295701

Characterization of Aerosol Surface Instruments in Transition Regime

Heejung Jung[1] and David B. Kittelson[2]

[1]*Department of MAE & LAWR, University of California, Davis, California, USA*
[2]*Department of Mechanical Engineering, University of Minnesota, Minneapolis, Minnesota, USA*

The primary purpose of this study is to measure the size- and composition-dependent responses of aerosol surface instruments designed to measure surface area related properties. Measurements were conducted in the range of 30–150 nm of mobility equivalent diameter, D_p. The responses of a LQ1-DC (a diffusion charger manufactured by Matter Engineering AG) and an EAD (a diffusion charger manufactured by TSI) to singlets (NaCl) particles are proportional to $D_p^{1.36}$ and $D_p^{1.13}$, respectively. The response of LQ1-DC agrees with Fuchs surface area, which is proportional to $D_p^{1.39}$ within 2.4% error. The response of the EAD is almost proportional to diameter, D_p. A PAS2000CE (Photoelectric Aerosol Sensor manufactured by EcoChem) gave both size and composition-dependent responses. For diesel particles produced at high engine loads, the response was nearly proportional to Fuchs surface area. However, at lighter engine loads, the response dropped sharply with decreasing D_p. Light engine loads are associated with high fractions of volatile particles that may suppress the photoemission response. The secondary purpose of this study is to investigate the difference in charging rate between singlets (NaCl particles) and agglomerates (diesel particles) by using diffusion chargers. Agglomerates (diesel particles at engine load 75%) acquire more charge than singlets (NaCl particles) by 15 and 17% for LQ1-DC and EAD, respectively.

INTRODUCTION

There is a growing concern about the environmental impact of particulate matter and increasing interest in metrics, other than particle-mass concentration, such as size fractionated mass, number concentration, and surface concentration. Some health studies suggest that the biological response is better correlated with surface concentration than with mass or number (Brown et al. 2000). The purpose of this study is to characterize the size-dependent response of surface instruments including diffusion chargers using Fuchs surface area. This study focuses on fast response measurement of surface area related properties of various particles including diesel agglomerates. Such agglomerates are an important component of ambient particulate matter, especially in urban areas.

Fast response instruments that respond to particle surface fall into two classes: Photoelectric Aerosol Sensors (PAS) and diffusion chargers. A PAS (PAS2000CE) (Kasper et al. 2000) manufactured by EcoChem Analytics, a diffusion charger (LQ1-DC) manufactured by Matter Engineering AG, and a diffusion charger (EAD, model 3070A) (Medved et al. 2000) manufactured by TSI were used for this study. These instruments all have a response time of 10 s or less.

The PAS was developed to mainly measure combustion generated particles because those particles show the highest photoemission among all particles in the environment (Burtscher 1992). The PAS response can give information about the surface of the particle, since photoemission is a phenomenon that takes place on the surface (Burtscher 1992). The photoelectric yield for diesel particles was investigated by Leonardi et al. (1993). Leonardi found that the yield is proportional to the 3rd power of the difference between photon and threshold energies for diesel particles. Burtscher et al. (1998) showed that the PAS response for diesel particles is proportional to the inverse of electrical mobility, 1/B.

Diffusion chargers have been widely used for various applications. The EAA (Electrical Aerosol Analyzer, TSI model 3030) employed a diffusion charger for size classification (Liu and Pui 1975). These days diffusion chargers are being used to measure active surface area (Kasper et al. 2000) or to monitor surface area of particles associated with health effect (Wilson et al. 2003).

CHARGING THEORIES

An understanding of the particle charging process is essential in the design of instruments for electrical classification of

Received 28 January 2005; accepted 11 July 2005.

The authors thank Dr. Michael R. Zachariah for useful comments. We gratefully acknowledge TSI, Matter Engineering AG, and EcoChem for the instruments. HJ is indebted to Dr. George Biskos for his comments. This work was partially funded by the CRC E-43 program. Their support is gratefully acknowledged.

Address correspondence to David B. Kittelson, Department of Mechanical Engineering, University of Minnesota, 111 Church St. SE, Minneapolis, MN 55455. E-mail: kitte001@umn.edu

particles by size, electrostatic precipitators for removal of hazardous particles, and instruments like those investigated in this study. This study focuses on using diffusion charging and photoemission charging to measure the surface area related aerosol properties.

Diffusion Charging

Among diffusion charging theories, Fuchs (1963) model is widely accepted for particles larger than 50 nm in diameter (Rogak and Flagan 1992). Rogak and Flagan (1992) pointed out that the differences among theories are more pronounced for smaller particles, although other measurements (Adachi et al. 1985) support using Fuchs charging theory for smaller particle sizes ($\leq$50 nm). Filippov (1993) carried out the comparison between Fuchs charging theory and Monte Carlo simulation. His comparison supports application of Fuchs charging theory down to 30 nm, which is the smallest size of interest in this study.

It is well known that the image force plays an important role for ultrafine particles. The image force depends on the dielectric constant of the particle. Keller et al. (2001), calculated the critical particle size at which the image force becomes important. They concluded that the image force is negligible for particles above 20 nm in diameter. Rogak and Flagan (1992) concluded that particles above 40 nm have negligible image forces. The effect of image forces should be negligible for particles above 30 nm in diameter, which is the range of our interest.

The particle charges (number of elementary charge units) acquired by a particle of diameter, D_p, is often expressed using a charging parameter, $N{\cdot}t$ product, where N means number concentration of ions and t means residence time of aerosol in the charging region of a diffusion charger. The charged fraction depends on the $N \cdot t$ product, particle size, and the ion-particle combination coefficient (Pui et al. 1988).

Photoemission Charging

Particles can be charged by UV light irradiation. Photoelectron emissions from particles occur when the photon energy is higher than the work function of the particle surface. Cardona and Ley (1978) defined the probability, Y, of the emission of an electron from a particle as a function of the photon energy ($h \cdot \nu$) and threshold Φ in the following Equation [1]:

$$Y = c(h\nu - \Phi)^x \ (h\nu > \Phi). \qquad [1]$$

For diesel particles (Leonardi 1991) $x = 3$ and c is a constant. Burtscher (1992) pointed out that soot particles show the highest photoemission of all the particles in the environment, whereas salt particles, most metal oxides, and water drops require much higher photon energy to emit electrons, implying high photo-threshold for these particles.

The efficiency of photoemission charging is much higher than diffusion charging, especially for ultrafine particles. However, the charge distribution in the ultraviolet chargers is still poorly understood as pointed out by Maisels et al. (2002). The emitted photoelectrons can recombine with the particles from which they were emitted or with other particles in the aerosol. This phenomenon is called recombination or back diffusion process of photoelectrons. If this occurs dominantly in the photoemission charger, the charging rate (in other words, the response of the instrument) drops significantly.

Maisels et al. (2002) studied the photo-charging process numerically and analytically for polydisperse one-component aerosol. They reported that concentrated aerosol would have bipolar charge distribution through the photo-charging process because the recapture of photoelectrons (recombination) is enhanced by a large particle concentration. The presence of negatively charged particles decreases the net current measured and the instrument response.

Ion Species for Diffusion Charging

Bricard et al. (1972) studied the diffusing ion species using α-^{210}Po radioactive source. They used artificial air and pure gas (Ar) with controlled humidity (1 $\sim$ 10,000 ppm). At low humidity (H_2O = 0.5 ppm), the dominant, small ionic species were O_2^+ in artificial air. Above a sufficiently high humidity (on the order of some ppm), they concluded the possible sequences of ions are $(H_3O)^+(H_2O)_n$, $NO_2^+(H_2O)_n$, $NO^+(H2O)_n$ in artificial air, and $(H_3O)^+(H_2O)_n$ series in Ar.

Davison and Gentry (1984) estimated the effect of moisture in the unipolar diffusion charging process. They concluded that the clusters of water molecules attach to the ions so that the mass of the ions increases, resulting in slower diffusion. They suggested that if the variation of ion mass significantly affects the charging rate, humidity and temperature might affect the operating characteristics of a TSI EAA (Liu and Pui 1975), which depends on diffusion charging to produce a well defined particle charge distribution.

Pui (1976) performed an extensive survey to find the most likely ion species in the diffusion charger. For positive ions, he concluded that the hydrated proton $H^+(H_2O)_6$ is the most probable ion under his experimental condition of 10% relative humidity. Pui (1976) pointed out there is no apparent difference in mobility of ions produced from different sources, such as α-^{210}Po, β-Tr, corona discharge, and so on. He also concluded that humidity and the age of ions do significantly influence mass and mobility of ions. The mean free path of $H^+(H_2O)_6$ in air was calculated using Maxwell-Chapmann-Enskog theory of molecular diffusion (Bricard 1948) as 14.5 nm by Pui et al. (1988). This extends the transition regime to much smaller size range compared to using the mean free path of air, 65 nm, at STP condition.

Fuchs Surface Area

The term Fuchs surface area was first introduced by Pandis et al. (1991) and defined for the surface area the epiphaniometer (Gäggeler et al. 1989) measures. Pandis et al. (1991) defined the

Fuchs surface area in a dimensionless quantity as follows;

$$S_{Fuchs} = \pi \left(\frac{D_p}{D_0} \right)^{x(D_p)} \quad [2]$$

where D_p is the mobility equivalent diameter, $D_0 = 1\ \mu$m, and $x(D_p)$ varies between 1 and 2, according to the regime of interest. $x(D_p)$ is determined by the Fuchs form of the coagulation coefficients using the experimental values of "coagulation" coefficients between lead atoms and the aerosol in the measurements done by the epiphaniometer.

Matter engineering AG (2001) defines the Fuchs surface area in a more complex form but more explicitly using the following equations according to regimes.

$$\begin{aligned} A_{Fuchs\_FM} &= \pi D_p^2 \\ A_{Fuchs\_CONT} &= 2\pi\lambda \cdot (A + Q) \cdot D_p \\ A_{Fuchs\_TR} &= \frac{\pi (A + Q) \cdot D_p^2}{\frac{D_p}{2\lambda} + \left(A + Q \cdot \exp\left(\frac{-b \cdot D_p}{2\lambda} \right) \right)} \end{aligned} \quad [3]$$

Here, D_p is the mobility equivalent diameter, λ is the mean free path of the diffusing species in the carrier gas, and A, b, Q are Cunningham fit parameters. A_{Fuchs_FM}, A_{Fuchs_CONT}, and A_{Fuchs_TR} are Fuchs surface area in free molecular, continuum, and transition regime, respectively. Their definition also considers the combination coefficients between ions and the particles. However, instead of using the combination coefficients values, which should be determined experimentally using specific instruments, they used the Cunningham slip correction factor that reflects empirical consideration of combination coefficients or mass transfer. The Fuchs surface area, as defined by Matter engineering AG (2001), should give the same area, if it is nondimensionalized, as defined by Pandis et al. (1991). The Fuchs surface area, defined by Matter engineering AG (2001), was derived in the appendix. It was done by extracting the surface area term from Stokes law.

To calculate Fuchs surface area using Equation [3], mean free path should be substituted in the equation. It should be noted that the definition of the mean free path should be consistent in transition regime because there are a variety of definitions in transition regime as Rader (1985) reviewed. The mean free path used in Cunningham slip correction factor (in other words, used in Fuchs surface area defined by Matter engineering AG) is defined using Chapman and Enskog's calculation (Davies 1945) following Maxwell's method (Jeans 1940).

Figure 1 shows Fuchs surface area as a function of mobility diameter using the equations in set [3]. As is shown in equation set [3], Fuchs surface area is proportional to D_p^2 in free molecular regime and it is proportional to D_p in continuum regime.

The size range between 30 and 150 nm corresponds to the size range containing most of the particle number and surface for typical diesel aerosols. It also corresponds to the size range where most of the surface area is found in atmospheric aerosols (Jaenicke 1998). The 30 nm lower limit of the measurement was selected to avoid significant diffusion loss and image forces.

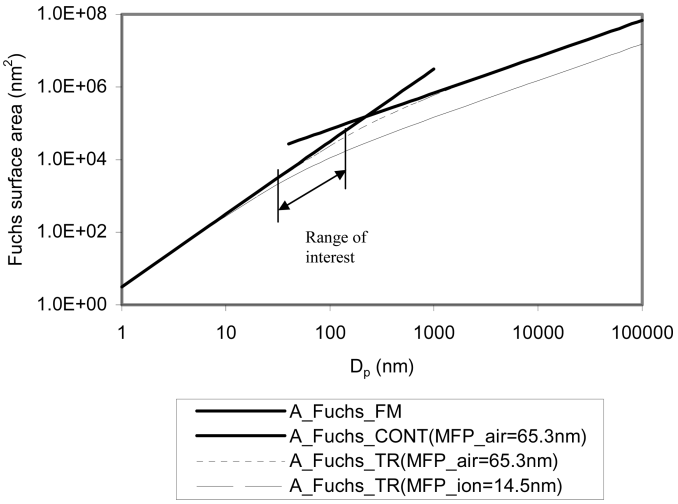

FIG. 1. Fuchs surface area as a function of particle size and mean free path of diffusing species.

EXPERIMENTAL

Aerosol Generation

A collision-type nebulizer system, which is similar to TSI model 3076, was used to generate NaCl aerosol. A turbo-charged 4.5L diesel engine manufactured by John Deere (Model 4045T) was used to generate diesel particles, which are mainly agglomerates. For this study, a standard EPA No. 2 on-road diesel fuel (300–500 ppm sulfur) and SAE15W-40 (John Deere TY6391) engine-lubricating oil was used. For diesel particles, a single-stage mini dilution tunnel (Abdul-Khalek et al. 1999) was used to dilute particles from the exhaust pipe at a ratio of 16∼23 to 1, according to the engine load condition. The 10% engine load (Torque = 40 N · m) at 1400 rpm and the 75% engine load (Torque = 300 N · m) at 1400 rpm were used to generate particles of different size and composition. The 10% load case is associated with a large soluble organic fraction and a high concentration of tiny particles in the nuclei mode region, while the 75% load case produces a lower soluble organic fraction and mainly larger particles in the accumulation mode diameter range (Ziemann et al. 2002). For the engine used in this study, VOF (Volatile Organic Fraction) was measured as follows: 60% VOF at 10% load, 30% VOF at 50%, and 15% VOF at 75% 1400 rpm.

Particle Size Selection

NaCl or diesel particles in the diameter range of 30–150 nm were used. A Differential Mobility Analyzer (DMA) was used to select monodisperse particles of a selected size for characterization of the surface instruments. Particles coming out of the DMA are all electrically charged, so a neutralizer was

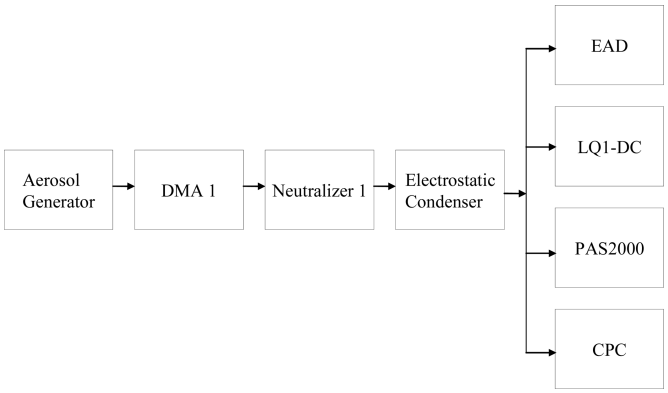

FIG. 2. Schematic diagram of the experimental setup.

used to bring the aerosol to a Boltzmann charge distribution, with the majority of the particles uncharged. Any charged particles were precipitated in the electrostatic condenser following the neutralizer so that only neutral particles were supplied to the EAD, LQ1-DC, PAS2000CE, and Condensation Particle Counter (CPC, TSI model 3025A). Care was taken for the flow lines split after electrostatic condenser to have the same diffusion losses. Figure 2 shows the experimental setup. Corrections were made to account for particles containing multiple charges passing through a DMA. Details are described in the Appendix.

Instruments

While the detailed inner structure of the aerosol surface instruments used in this study can be found in the user manuals for each instrument, the authors would like to point out a few important features of these instruments. While the LQ1-DC (Matter Engineering AG, 2001) has a similar structure to the diffusion charger used in the EAA (Liu and Pui 1975), the charging region of the EAD (TSI 2002) is set up in a counter flow configuration for better charging. It is relatively more difficult to quantify $N \cdot t$ product for the EAD, because the flow is not laminar and the boundaries of the charging region are poorly defined.

In a PAS, charged particles flow through a short tube before entering a filter component. Within the tube, where irradiation-free and only recapturing can occur, a small voltage is applied to remove negative ions and electrons to minimize the recapture effect (EcoChem Analytics 2001).

RESULTS AND DISCUSSION

Characterization of Diffusion Chargers Using NaCl Particles

Figure 3 shows the size dependency of the response for the diffusion chargers using NaCl particles. The response of each diffusion charger per-unit Fuchs surface area is calculated by dividing the response of a diffusion charger by total Fuchs surface area,($A_{Fuchs} \cdot CPC\,counts$), based on the mean free path of

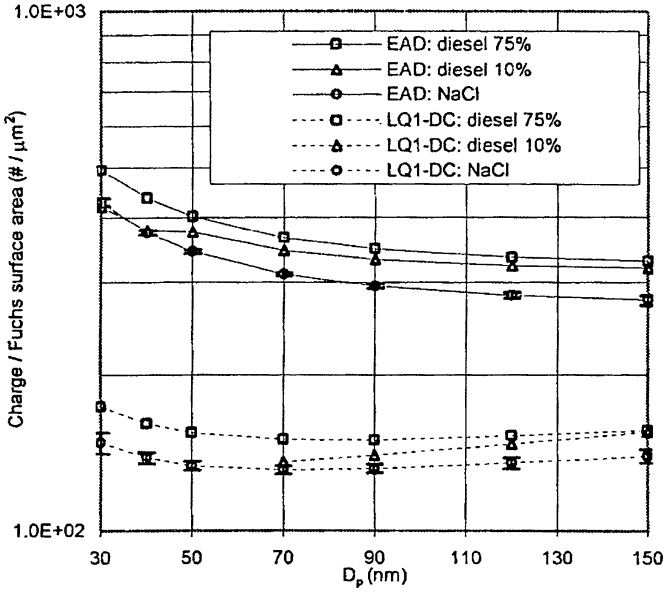

FIG. 3. The response of diffusion chargers (LQ1-DC and EAD) for diesel agglomerate particles compared to NaCl particles, as a function of particle size. Engine operated at 1400 rpm with variable loads.

14.5 nm. It shows the net response of a diffusion charger per unit Fuchs surface area. LQ1-DC data show a nearly constant value of LQ1-DC response/total Fuchs surface area meaning the instrument responds to the Fuchs surface area, whereas the response of EAD becomes larger than expected from Fuchs theory, as the particle size gets smaller. Liu and Pui (1975) showed the charging efficiency of the EAA charger as a function of particle size in Figure 11 of their paper. The plot follows the typical Fuchs surface area curve, which is shown at Figure 1 of this paper. This indicates that the EAA charger, which has similar inner structure to that of the LQ1-DC, also correlates with Fuchs surface area.

The different size dependency of EAD compared to that of LQ1-DC might come from their unique design of charging region (or mixing region for ions and aerosol). The counter-flow jets cause turbulence in the charging region (Medved et al. 2000). The reason for higher charging rate of EAD for small-sized particles compared to large-sized particles is not identified in this study.

In the size range from 30 to 150 nm, Fuchs surface area is proportional to $D_p^{1.39}$, as Figure 1 shows when the mean free path of diffusing species is 14.5 nm.

Figure 4 shows the charge per particle of diffusion chargers for NaCl aerosol, as a function of particle size. The LQ1-DC response is proportional to $D_p^{1.36}$. This exponent is close to that of Fuchs' within about 2%. This means that LQ1-DC responds to the Fuchs surface area in the range between 30 and 150 nm. Ntziachristos et al. (2001) obtained $D_p^{1.37}$ proportionality for ASMO (A diffusion charger manufactured by Dekati), which is consistent with the result of the current study.

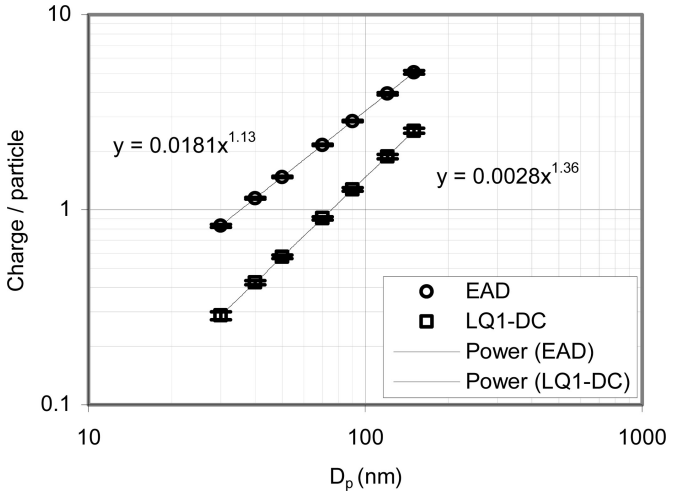

FIG. 4. Charge per particle for LQ1-DC and EAD (for NaCl aerosol).

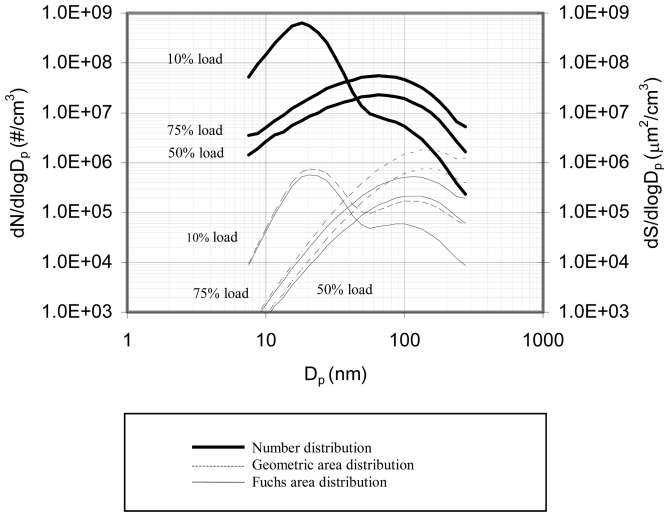

FIG. 5. Typical size distribution of the diesel exhaust particles used for the experiments: Number distribution, Geometric surface area (πD_p^2) distribution, and Fuchs surface area distribution. Engine operated at 1400 rpm with variable loads.

The EAD response per unit CPC count is proportional to $D_p^{1.13}$. This is shown in Figure 4 suggests that the EAD does not respond to Fuchs surface area unless the effective mean free path of the charging species is much smaller, about 4 nm, which is unlikely. Thus, the charging process in the EAD may be more complex than simple diffusion charging.

Characterization of Diffusion Chargers Using Soot Agglomerates

For the diesel engine used in these tests, particles at high engine load (75%) are mainly agglomerates over the whole size range and mostly found in accumulation mode, whereas particles at light engine load (10%) are composed of both nuclei mode and accumulation mode particles (Ziemann et al. 2002). The nuclei mode particles are mainly composed of volatile organics for sizes below ∼30 nm. The nuclei mode particles typically lay within 3∼30 nm, but they tend to merge into the accumulation mode under very light engine load. The accumulation mode particles are agglomerates composed of mainly solid carbonaceous materials (Kittelson 1998). Figure 5 shows typical size distributions of diesel exhaust particles used in the experiment. They are measured using a Scanning Mobility Particle Sizer (SMPS) and corrected for a dilution ratio. In surface-weighted size distributions, one can notice the nuclei mode particles have a comparable surface area concentration to that of accumulation mode particles. Figure 3 shows the responses per Fuchs surface area for diesel agglomerates compared to the NaCl particles for LQ1-DC and EAD, respectively. Soot particles at 75% engine load acquire about 15 and 17% more charge, compared to NaCl particles, over the whole size range of the experiment for LQ1-DC and EAD, respectively. This is consistent with the idea that agglomerates become more highly charged because charge can be distributed over larger area in the agglomerate compared to the spherical particle of the same mobility size. Laframboise and Chang (1977) showed that prolate spheroids become more highly charged than spherical particles of the same mobility.

For diesel particles generated at 10% engine load, the response of the larger size accumulation mode particles is similar to that of diesel particles generated at 75% engine load. This is because most accumulation mode particles are agglomerates. The particles in the nuclei mode, particles smaller than 50 nm, are not agglomerates. Therefore, those nuclei mode particles follow the response of NaCl more closely.

Sakurai et al. (2003) measured volatility of the particles in the nuclei mode. They found there are two kinds of PM in the nuclei mode: more volatile PM and less volatile PM. More volatile PM is mainly composed of volatile organics, whereas less volatile PM is composed of carbonaceous particle with volatile organics coated on the surface. Their study shows that as particle size gets smaller, the fraction of more volatile PM increases in the nuclei mode.

Rogak and Flagan (1992) studied the bipolar diffusion charging of spherical particles and agglomerates. They measured the uncharged fraction of PSL, $(NH_4)_2SO_4$, and TiO_2 particles. In their study, the agglomerates had a higher charged fraction than the spherical particles. In other words, the agglomerates acquired more charge than the spherical particles with the same mobility size. They reported an approximate 10% increase of charging-equivalent diameter in the bipolar diffusion charging process for agglomerates in the size range of $100 < D_p < 800$ nm. The 10% increase in equivalent diameter will result in a 14% increase in charging rate according to the $D_p^{1.39}$ proportionality of Fuchs surface area, in the size range of this study. It shows excellent agreement with the result of the current study.

Figure 6 shows charge per particle curves for diesel particles generated at 75% load in comparison with several charging models. An arbitrary constant was multiplied to Fuchs surface area

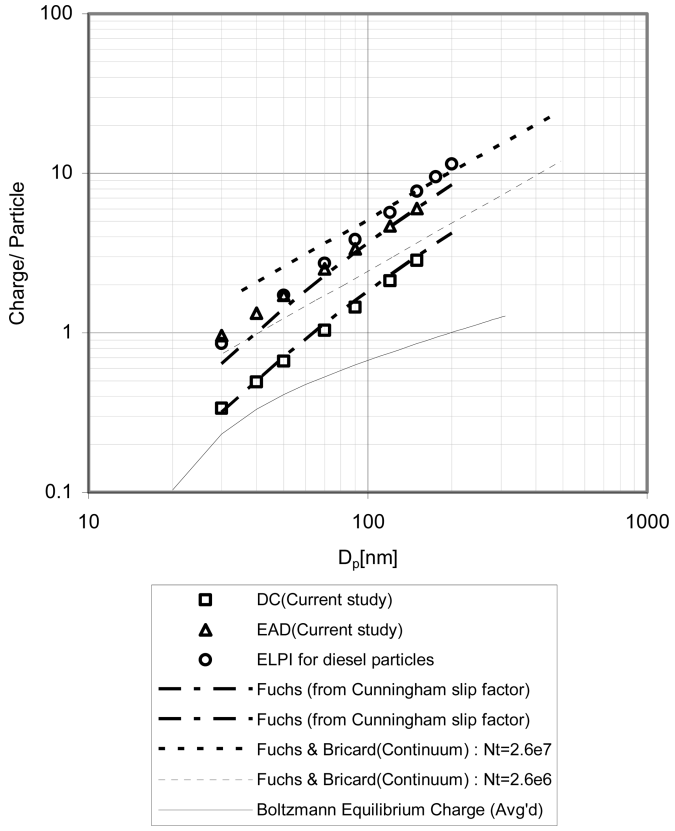

FIG. 6. Charge per particle (Comparison with prior studies): (1) ELPI for diesel particles by Ntziachristos (2001), (2) Fuchs (1947), (3) Bricard (1948), and (4) current study for diesel particles generated at 75% load.

curves to compare it to other charging models and experimental data. The charge per particle curve of LQ1-DC matches well with Fuchs surface area curve, whereas that of EAD has a lower slope than Fuchs surface area curve.

While there is no data available in the literature on the size-dependent responses of the PAS, to the authors' knowledge, there have been many prior studies (Filippov 1993; Liu and Pui 1975; Pui et al. 1988) on size-dependent responses of diffusion chargers. However, we could not directly compare our results on the response of the diffusion charger with most of the prior studies, because $N \cdot t$ products were not given for instruments used in this study. For this reason, there is an offset between the response of the LQ1-DC and the ELPI in Figure 6. The charge per particle for diesel agglomerates of the charger used in the ELPI (Electrical Low Pressure Impactor) by Ntziachristos et al. (2001) was higher than for the other instruments reported in Figure 6. In addition, most prior studies overlooked the fact that the response of a diffusion charger can be correlated with Fuchs surface area.

The epiphaniometer (Gäggeler et al. 1989) also measures Fuchs surface area. The epiphaniometer works by using the attachment of ^{211}Pb onto the aerosol particles. The α-detector counts the number of ^{211}Pb atoms attached onto the particles. The lead atoms are hydrated after they appear by radioactive chain decay starting from ^{227}Ac. The hydrated lead atoms are transported to the particles mainly by diffusion; the response of the epiphaniometer is known to be proportional to Fuchs surface area (Pandis et al. 1991). Shi et al. (2001) compared Fuchs surface area, measured by the epiphaniometer, to that measured by SMPS for NaCl, $(NH_4)_2SO_4$, and carbon agglomerates. He conducted experiments similar to the current study using an epiphaniometer instead of a diffusion charger. Their results show that there is no difference in the response of an epiphniometer between singlet (such as NaCl) and carbon agglomerates for a given mobility diameter. Rogak et al. (1991) also compared transfer rates of ^{211}Pb onto particles using the epiphaniometer for $(NH_4)_2SO_4$, PSL, and TiO_2 agglomerates. They concluded that spherical shape particles and agglomerates with the same mobility have nearly the same transfer rate of ^{211}Pb. These results suggest that the rate of diffusion of neutral species (such as ^{211}Pb in epiphaniometer) onto agglomerates is the same as that for spherical particles of the same mobility diameter, within experimental error. However, our results indicate the diffusion of ions onto agglomerates is slightly larger than onto the spherical particle of the same mobility diameter most likely as the result of electrostatic effects.

Characterization of a Photoelectric Aerosol Sensor

Figure 7 shows the PAS2000CE response per unit Fuchs surface area. DMA size-classified diesel particles produced at 10, 50, and 75% engine load at 1400 rpm were used to characterize the instrument. NaCl particles are weak photo emitters, so could not be used. It is known that PAS response changes as the chemical composition of the particle changes (Kasper et al. 2000). It gives a weak response to particles with layers, which contain moisture or volatile organics. Figure 5 shows size distributions of diesel particles used for the experiment. The highest peak, around 30 nm at 10% engine load, is known as the nuclei mode. It is known that the particles in nuclei mode from light engine load of about 10% consist mainly of volatile organics and larger

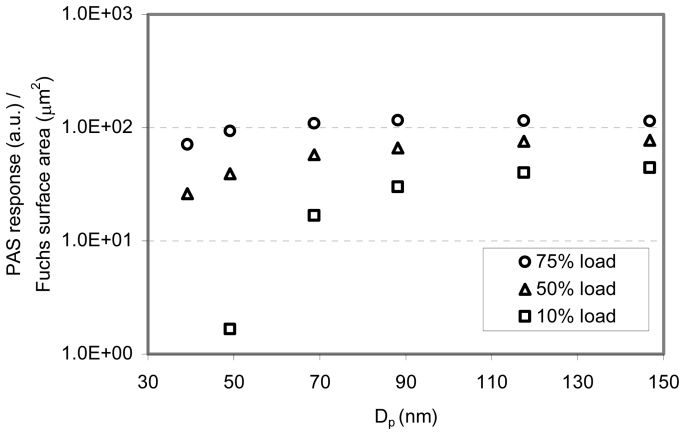

FIG. 7. The response of PAS2000CE for diesel agglomerate particles. Engine operated at 1400 rpm with variable loads.

particles are coated with volatile organic material (Tobias et al. 2001; Ziemann et al. 2002).

The PAS2000CE response changes as the chemical composition of the particles changes with the engine load, as shown in Figure 7. Generally, the lower the engine load, the higher the VOF (Volatile Organic Fraction) of the particle due to the lower combustion and exhaust temperature in the diesel engine (Kittelson 1998). Particles from the higher engine load gave higher PAS response per unit Fuchs surface area due to the different chemical composition and lack of VOF compared to particles of lower engine load. Particles smaller than 80 nm, at 10% engine load, gave very weak PAS responses compared to particles of the same size at higher engine loads. This results because the fraction of volatile particles, which do not respond to PAS, increases as the particle size gets smaller in light engine load.

The higher PAS response at higher engine load is most likely due, in part, to the change in light absorption near the surface, where less volatile materials are present, as Burtscher (1992) pointed out. Steiner and Burtscher (1993) showed that desorption of volatile material from diesel particles leads to higher PAS signal. It is consistent with the current study since, at a higher engine load, less volatile material is condensed on the surface of diesel particles. The smaller size particles in 10% engine load have a weaker PAS response because of the increase in volatile PM fraction.

Diesel particles used in this study were extensively characterized by Park et al. (2004) using the same engine at 50% engine load. A TEM analysis was used to measure the primary particle size as 32 ± 7 nm. This analysis also measured the size-dependent shape factor, as well as the inherent density of diesel particles.

CONCLUSION

Three instruments to measure surface area related properties of particles have been characterized. Experiments conducted using size-classified, roughly spherical (NaCl) particles in 30–150 nm diameter showed that LQ1-DC gives a response that is proportional to Fuchs surface area for mean free path of diffusing species of ~15 nm. The EAD response is proportional to $D_p^{1.13}$ in the same particle size range. It has a flatter response than LQ1-DC. Since EAD gives a better response to smaller particles than LQ1-DC, the EAD is more sensitive to nuclei mode particles. The different response behavior, compared to Fuchs surface area, may come from the unique design of the counter-flow mixing chamber. The responses of the LQ1-DC and EAD to size-classified diesel agglomerates were 15 and 17 % higher than to NaCl particles of the same mobility diameter. This indicates higher unipolar charging efficiencies for agglomerates and is consistent with earlier work (Rogak and Flagan 1992).

A PAS2000CE (Photoelectric Aerosol Sensor manufactured by EcoChem) gave both size- and composition-dependent responses. For diesel particles produced at high engine load, the response was nearly proportional to Fuchs surface area. However, at lighter loads, the response dropped very sharply with decreases in D_p. Light loads are associated with high fractions of volatile particles which may suppress the photo emission response.

REFERENCES

Abdul-Khalek, I., Kittelson, D. B., and Brear, F. (1999). The Influence of Dilution Conditions on Diesel Exhaust Particle Size Distribution Measurements. SAE TECHNICAL PAPER SERIES: 1999-01-1142.

Adachi, M., Kousaka, Y., and Okuyama, K. (1985). Unipolar and Bipolar Diffusion Charging of Ultrafine Aerosol Particles, *J. Aerosol Sci.* 16:109–123.

Bricard, J. (1948). Életricité Atmosphérique, *C. R. Acad. Sci. Paris* 226:1536–1538.

Bricard, J., Cabane, M., Madelaine, G., and Vigla, D. (1972). Formation and Properties of Neutral Ultrafine Particles and Small Ions Conditioned by Gaseous Impurities of the Air, *J. Colloid Interface Sci.* 39(1):42–58.

Brown, L. M., Collings, N., Harrison, R. M., Maynard, A. D., and Maynard, R. L. (2000). Ultrafine Particles in the Atmosphere, *Phil. Trans. Roy. Soc. London Series A* 358(1775):2561–2797.

Burtscher, H. (1992). Measurement and Characteristics of Combustion Aerosols with Special Consideration of Photoelectric Charging and Charging by Flame Ions, *J. Aerosol Sci.* 23(6):549–595.

Burtscher, H., Kunzel, S., and Huglin, C. (1998). Characterization of Particles in Combustion Engine Exhaust, *J. Aerosol Sci.* 29(4):389–396.

Cardona, M., and Ley, L., Eds. (1978). *Topics in Applied Physics.* Photoyield Near Threshold. Berlin, Springer.

Davies, C. N. (1945). Definitive Equations for the Fluid Resistance of Spheres, *Proc. Phys. Soc.* 57(322):259–270.

Davison, S. W., and Gentry, J. W. (1984). Modeling of Ion Mass Effects on the Diffusion Charging Process, *J. Aerosol Sci.* 15(3):262–270.

EcoChem Analytics (2001). User Manual of PAS 2000CE.

Filippov, A. V. (1993). Charging of Aerosol in the Transition Regime, *J. Aerosol Sci.* 24:423.

Fuchs, N. A. (1947). The Charges on the Particles of Aerocolloids. Investiya Acad. Nauk USSR, *Ser. Geogr. Geophys.* 11:341.

Fuchs, N. A. (1963), *Geofis. Pura Appl.* 56:185.

Gäggeler, H. W., Baltensperger, U., Emmenegger, M., Jost, D. T., Schmidt-Ott, A., Haller, P., and Hofmann, M. (1989). The Epiphaniometer, A New Device for Continuous Aerosol Monitoring, *J. Aerosol Sci.* 20(5):557–564.

Jaenicke, R., Ed. (1998). *Atmospheric Particles*. Wiley, New York.

Jeans, J. (1940). *An Introduction to the Kinetic Theory of Gases*. Cambridge University Press, London.

Kasper, M., Matter, U., and Burtscher, H. (2000). NanoMet: On-Line Characterization of Nanoparticle Size and Composition. SAE TECHNICAL PAPER SERIES:2000-01-1998.

Keith, L., Crummett, W., Deegam, J., Libby, R., Taylor, J., and Wentler, G. (1983). Principles of Environmental Analysis, *Anal. Chem.* 55(14):2210–2218.

Keller, A., Fierz, M., Siegmann, K., Siegmann, H. C., and Filippov, A. V. (2001). Surface Science with Nanosized Particles in a Carrier Gas, *J. Vac. Sci. Technol. A.* 19(1):1–8.

Kittelson, D. B. (1998). Engines and Nanoparticles: A Review, *J. Aerosol Sci.* 29(5/6):575–588.

Laframboise, J. G., and Chang, J. (1977). Theory of Charge Deposition on Charged Aerosol Particles of Arbitrary Shape, *J. Aerosol Sci.* 8:331–338.

Leonardi, A. (1991). Feinste Schwebeteilchen aus Dieselmotoren. Zürich, ETH. Diss.

Leonardi, A., Burtscher, H., and Siegmann, H. C. (1993). Size-Dependent Measurement of Aerosol Photoemission From Particles in Diesel Exhaust, *Atmos. Environ.* 27A(8):1251–1254.

Liu, B. Y. H., and Pui, D. Y. H. (1975). On the Performance of the Electrical Aerosol Analyzer, *J. Aerosol Sci.* 6:249–264.
Maisels, A., Jordan, F., and Fissan, H. (2002). Dynamics of the Aerosol Particle Photocharging Process, *J. Appl. Phys.* 91:3377.
Matter Engineering AG. (2001). Operating Manual of LQ1-DC.
Medved, A., Dorman, F., Kaufman, S. L., and Pocher, A. (2000). A New Corona-Based Charger For Aerosol Particles, *J. Aerosol Sci.* 31(S.1):616–617.
Ntziachristos, L., Giechaskiel, B., and Samaras, Z. (2001). Calibration of Dekati's Automotive Surface Monitor-"ASMO, LAT Report, No: 0117, Thessaloniki School of Engineering, Aristotle University.
Pandis, S. N., Baltensperger, U., Wolfenbarger, J. K., and Seinfeld, J. H. (1991). Inversion of Aerosol Data from the Epiphaniometer, *J. Aerosol Sci.* 22(4):417–428.
Patschull, J., and Roth, P. (1992). Charge and Size Distribution of Particles Emitted From a DI-Diesel Engine, *J. Aerosol Sci.* 23:S229–S232.
Pui, D. Y. H. (1976). Experimental Study of Diffusion Charging of Aerosols. Mechanical Engineering Department. Minneapolis, University of Minnesota, Ph.D thesis.
Pui, D. Y. H., Fruin, S., and McMurry, P. H. (1988). Unipolar Diffusion Charging of Ultrafine Aerosols, *Aerosol Sci. Technol.* 8:173–187.
Rader, D. J. (1985). Application of the Tandem Differential Mobility Analyzer to Studies of Droplet Evaporation and Growth. Mechanical Engineering. Twin Cities, University of Minnesota. Ph.D thesis.
Rogak, S. N., Baltensperger, U., and Flagan, R. C. (1991). Measurement of Mass Transfer to Agglomerate Aerosols, *Aerosol Sci. Technol.* 14:447–458.
Rogak, S. N., and Flagan, R. C. (1992). Bipolar Diffusion Charging of Spheres and Agglomerate Aerosol-Particles, *J. Aerosol Sci.* 23:693.
Sakurai, H., Park, K., McMurry, P. H., Zarling, D. D., Kittelson, D. B., and Ziemann, P. J. (2003). Size-Dependent Mixing Characteristics of Volatile and Non-Volatile Components in Diesel Exhaust Aerosols, *Environ. Sci. Technol.* 37:5487–5495.
Shi, J. P., Harrison, R. M., and Evans, D. (2001). Comparison of Ambient Particle Surface Area Measurement by Epiphaniometer and SMPS/APS. *Atmospheric Environment* 35:6193–6200.
Steiner, D., and Burtscher, H. (1993). Studies on the Dynamics of Adsorption and Desorption from Combustion Particles, by Temperature Dependent Measurement of Size, Mass and Photoelectric Yield. *Water, Air and Soil Pollution* 68:159–176.
Tobias, H. J., Beving, D. E., Ziemann, P. J., Sakurai, H., Zuk, M., McMurry, P. H., Zarling, D., Waytulonis, R., and Kittelson, D. B. (2001). Chemical Analysis of Diesel Engine Nanoparticles Using a Nano-DMA/Thermal Desorption Particle Beam Mass Spectrometer, *Environ. Sci. Technol.* 35:2233–2243.
TSI (2002). Model 3070A Electrical Aerosol Detector Instruction Manual.
White, H. J. (1951). Particle Charging in Electrostatic Precipitation, *Trans. Am. Inst. Elec. Engrs.* 70:1186–1191.
Willeke, K., and Baron, P. A., Eds. (1992). *Aerosol Measurement: Principles, Techniques, and Applications*. Wiley. New York.
Wilson, W. E., Han, H. S., Stanek, J., Turner, J., and Pui, D. Y. H. (2003). Deposition of Particle Surface Area in the Human Respiratory Tract: Relation to Particle Concentration (Number, Surface Area and Volume) and to the "Active" Surface Area as Measured by a Diffusion Charger. AAAR 2003, Anaheim, CA.
Ziemann, P. J., Sakurai, H., and McMurry, P. H. (2002). Chemical Analysis of Diesel Nanoparticles using a Nano-DMA/Thermal Desorption Particle Beam Mass Spectrometer, CRC: Project No. E-43-4, Final Report.

APPENDIX

Multiple Charge Correction

When a DMA selects particles of certain cut-size, the selected particles contain multiply charged particles. These multiply charged particles have the same electrical mobility, but different sizes. Therefore neutralized particles supplied to surface aerosol instruments shown in Figure 2 includes larger particles, which were originally multiply charged when they passed through the DMA. The fraction of larger particles supplied to surface aerosol instruments was measured using an experimental setup shown in Figure A-1. Neutralizer 2 re-applied a Boltzmann charge distribution to the neutral particles. Particle size distributions were then measured by DMA 2, as shown in Figure A-2. This gave the ratio of singly and multiply charged particles. In Figure A-2, the first peak on the left shows particles charged the same in DMAs 1 and 2 (e.g., +1, +1; +2, +2; +3, +3; . . .) and the second peak in the middle shows particles charged doubly when passing through DMA 1 but charged singly when passing through DMA 2 (+2, +1), where (+A, +B) stands for particle charge number at DMA 1 and 2 respectively. It was assumed that all particles contained either single or double charges. For example, we assumed that the first peak was composed of (+1, +1) and (+2, +2) since the fraction of more than doubly charged particles were negligible from our measurements as shown in Figure A-2. Since the Boltzmann charge distribution was re-applied to the particles, as shown in Figure A-1, it was possible to obtain the fractions of singly and doubly charged particles supplied the aerosol instruments from the ratio between first peak and second peak in Figure A-2. Fractions of singly and doubly charged particles supplied to the aerosol instruments were obtained for every initial size selection by DMA 1 for NaCl and diesel aerosol at 75% load. It was assumed that particles generated at 50% and 10% load have the same multiple charge fraction as those generated at 75% load for particles larger than 50 nm, as the shape of accumulation modes were very similar as shown in Figure 5. It was found that the multiple charge fractions were negligible for 30 and 40 nm particles at 10% load. For this reason, these data were excluded from the least squares fitting discussed in the following section. In other words, no multiple charge correction was necessary for this experimental condition.

From the Fuchs area curve it was assumed that the response of aerosol surface instruments can be expressed as $a \cdot D_p^b$ in the transition regime, where a is a constant. The response of the aerosol surface instruments was normalized by the particle number concentration, and can be expressed as follows:

$$\text{Response of aerosol surface instruments/ particle number concentration} = a \cdot (f_{Dp+1} \cdot D_{p+1}^b + f_{Dp+2} \cdot D_{p+2}^b) \quad \text{[A-1]}$$

where f is the fraction, +1 singly and +2 doubly charged particles. By running the least squares method for all data at different size selections, the values of a and b for each instrument and each aerosol used in this study were determined. The R^2 values were high ($R^2 > 0.98$) for these fittings, which implies that the fitting correlates well with the data. This correction was used in all figures showing the response of diffusion chargers.

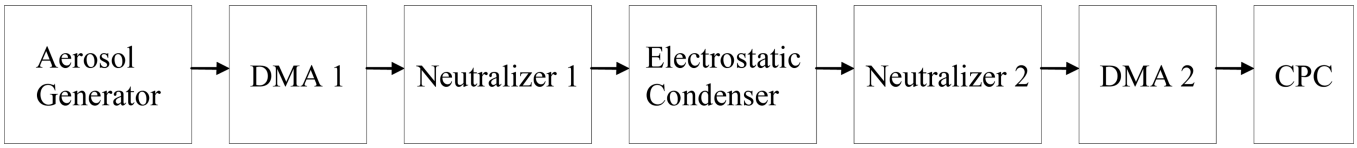

FIG. A-1. Schematic diagram of the experimental setup for multiple charge correction.

LOD (Limit of Detection) and LOQ (Limit of Quantification) of the Diffusion Chargers

The background noise level was measured for 5 hours to determine the LOD and LOQ of the diffusion chargers. To determine background noise level, absolute filters were installed at the inlet of the instruments. Willeke and Baron (1992) defined the LOD of a measurement as the value 3σ above the mean of the background distribution. LOQ is defined as the value 10σ above the mean of the background distribution (Keith et al. 1983).

The LOD and LOQ were obtained for both LQ1-DC and EAD. For convienience, they are plotted in terms of particle number concentrations in Figure A-3. The results show that both EAD and LQ1-DC have about the same LOD and LOQ. To assure the validity of the data, the measurements were carried out only for concentrations higher than LOQ. The LQ1-DC showed some long-term electrical zero drift. The zero of LQ1-DC was corrected every 5 minutes but the drift resulted in larger error bounds than expected. The frequent zero correction minimized any uncertainty in the measurements. Consequently, the measurement error bound of LQ1-DC is larger than the EAD measurement shown in Figure 3.

Humidity versus Response of Diffusion Chargers

The Relative Humidity (RH) of the Diesel aerosol streams was lowered by dilution with filtered and dried air. The RH of the nebulized aerosol streams, such as NaCl aerosol, was lowered by passing the streams through two diffusion driers prior to the DMA for size selection (This is not shown in Figure 3 to prevent the complication of the schematic diagram). Since the ratio of the aerosol sheath air to sample air was 10:1, the estimated RH of size selected aerosol in the charging region was always lower than 10% considering both dilution in the DMA and prior drying. Under extremely low RH levels such as in Bricard et al.'s (1972) study, the extent of hydration of the proton would be less than $(H_2O)_6$ and under humid conditions, the extent of hydration of proton would be more than $(H_2O)_6$ (Pui 1976). However, very repeatable data were observed in all experiments where humidity was controlled as described above. Furthermore, it was found that the response of the diffusion chargers correlated well with Fuchs surface area assuming $H^+(H_2O)_6$ is the most abundant species. This confirms that our assumption is reasonable for every experimental condition.

The silica gel that was used to dry the filtered air for the DMA and dilution was renewed daily at the beginning of every experiment. When this renewal of the silica gel was not done, fluctuations in the response of the diffusion chargers were observed, which correlated to the RH of the aerosol stream (data not shown). Error bars in Figure 3 and 4 shows the extent of the repeatibility of LQ1-DC and EAD responses.

Fuchs Surface Area

The following series of equations show how Matter engineering AG (2001) defined Fuchs surface area. The first equation is a Stokes equation. From there, A_{Fuchs_TR} can be obtained by

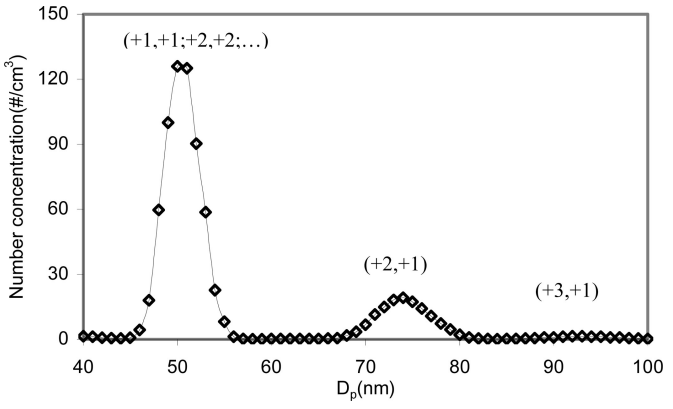

FIG. A-2. Multiple charge distribution (Size distribution measured at DMA 2 for 50 nm initial size selection at DMA 1 using a setup at Figure A-1).

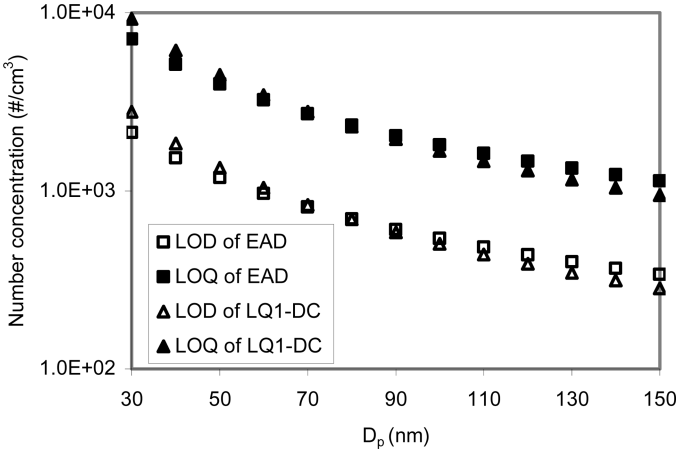

FIG. A-3. Limit of Detection (LOD) and Limit of Quantification (LOQ) of the diffusion chargers as a function of particle mobility diameter.

expressing $F_{drag} = \text{constant} \cdot \text{surface area} \cdot \text{velocity}$.

$$\begin{aligned} F_{drag\_TR} &= \frac{3\pi\eta V D_p}{C_c} \\ &= \frac{3\pi\eta V D_p}{1 + \frac{2\lambda}{D_p}\left(A + Q \cdot \exp\left(\frac{-b \cdot D_p}{2\lambda}\right)\right)} \\ &= \frac{3\pi\eta V D_p^2}{\left(2\lambda\left(\frac{D_p}{2\lambda} + A + Q \cdot \exp\left(\frac{-b \cdot D_p}{2\lambda}\right)\right)\right)} \\ &= A_{Fuchs\_TR} \cdot \frac{3\eta V}{2\lambda(A + Q)} \end{aligned} \quad \text{[A-2]}$$

F_{drag_CONT} and F_{drag_FM} can be derived from two limiting cases of the F_{drag_TR}, as illustrated below.

$$\begin{aligned} F_{drag\_CONT} &= 3\pi\eta V D_p \\ &= A_{Fuchs\_CONT} \cdot \frac{3\eta V}{2\lambda(A + Q)} \quad \text{when } D_p \gg \lambda \end{aligned}$$

$$\begin{aligned} F_{drag\_FM} &= \frac{3\pi\eta V D_p^2}{2\lambda(A + Q)} \\ &= A_{Fuchs\_FM} \cdot \frac{3\eta V}{2\lambda(A + Q} \quad \text{when } D_p \ll \lambda \end{aligned} \quad \text{[A-3]}$$